The impact of building operations on urban heat/cool islands under urban densification: a comparison between naturally-ventilated and air-conditioned buildings

Manuscript submitted to Applied Energy, Oct 2018

The impact of building operations on urban heat/cool islands under urban densification: a comparison between naturally-ventilated and air-conditioned buildings

Shuangping Duan[1,2], Zhiwen Luo[2,*], Xinyan Yang[3], Yuguo Li[4]

1. Department of Civil Engineering and Architecture, Southwest University of Science and Technology, Mianyang, China
2. School of the Built Environment, University of Reading, Reading, United Kingdom
3. China Academy of Building Research, Beijing, China
4. Department of Mechanical Engineering, University of Hong Kong, Hong Kong

Word count of abstract: **213**

Word count of text: **6647**

*Correspondence author:

Dr Zhiwen Luo, School of the Built Environment, University of Reading, United Kingdom

Email: z.luo@reading.ac.uk

Abstract

Many cities are suffering the effects of urban heat islands (UHI) or urban cool islands (UCI) due to rapid urban expansion and numerous infrastructure developments. This paper presents a lumped urban-building thermal coupling model which captures the fundamental physical mechanism for thermal interactions between buildings and their urban environment. The benefits of the model are its simplicity and high computational efficiency for practical use in investigating the diurnal urban air temperature change and its asymmetry in a city with both naturally-ventilated (NV) and air-conditioned (AC) buildings. Our model predicts a lower urban heat island and higher urban cool island intensity in a city with naturally-ventilated buildings than for a city with air-conditioned buildings. During the urban densification (from a low-rise, low-density city to a high-rise, high-density one), the increases in the time constant and internal heat gain give rise to asymmetric warming phenomena, which become more obvious in a city with air-conditioned buildings rather than naturally-ventilated ones. Unlike previous studies, we found that a low-rise, low-density city experiences a stronger urban cool island effect than a high-rise, high-density city due to less heat being emitted into the urban atmosphere. The urban cool/heat island effect will firstly increase/decrease, and then rapidly decrease/increase and ultimately disappear/dominate with increasing time constant in the process of urbanization/urban densification.

Keywords: Natural ventilation; urban heat island; urban cool island; urban morphology; Urbanization

1. Introduction

Due to socioeconomic development, increasing population and greater migration from rural to urban areas will give rise to large-scale urban expansion [1]. Urbanization results in the creation of urban heat islands (UHI), which involve a higher air temperature in a city than that in rural areas, especially at night time [2-3]. In a study of 38 U.S. cities, Imhoff *et al.* [4] found that the annual urban temperature was on average 2.9℃ warmer than surrounding areas in all biomes except those with arid and semiarid climates. In London, the maximum temperature difference between the urban and rural areas could reach 8.6℃ in clear-sky weather conditions with wind velocities below 5ms^{-1} [5-6]. An UHI intensity of 2.7℃~10℃ was observed in Athens, Greece [7]. Nevertheless, the urban air temperature could also be lower than the rural air temperature in some places or under certain meteorological conditions, which gives rise to the urban cool island (UCI) phenomenon [8-12]. The UCI intensity has been observed to be higher during the day than the night in summer and the opposite is true in winter [13-14]. Cohen *et al.* [13] found a maximum air UCI intensity of 3.8℃ in summer. Both UHI and UCI have a great impact on the energy demand [15-17] as well as the outdoor air quality of a city [18]. A UHI could lower the heating demand during winter and increase the building energy consumption for cooling in summer, while a UCI has the opposite effect. Meanwhile, the energy consumption of a city affects the pollutant concentration over urban areas.

There are many reasons contributing to the development of UHI and UCI. One of the important contributors is the heat stored by a huge thermal mass such as the man-made infrastructure in the city. The heat that is absorbed by the buildings and roads during the daytime will be re-emitted into the atmosphere during the night, leading to a UHI effect at night and a UCI effect during daytime [12]. In addition, the waste heat emissions released by building ventilation and air conditioning systems in summer can contribute to an increase in UHI intensity [19]. However, urban green spaces could lead to a UCI effect [20-21]. Although a UHI and UCI can co-exist during the course of the day, this is less explained and studied. In the process of urbanization, an increase in the building density and building height brings great changes in urban green spaces, urban thermal mass, anthropogenic heat, internal gain and so on, which will determine whether the UHI and UCI phenomena can coexist and their respective intensities.

There are basically two types of research coupling urban and building thermal simulations. One is the one-way coupling, where the urban meteorological data were directly used as the inputs for building energy simulation. Zinzi *et al* (2018) directly used the meteorological information measured at rural and urban sites in Italy to drive the building energy modelling to understand the variations of building heating and cooling loads on different sites [22]. An increase of 57% cooling degree days was observed in urban centre compared with that in rural area. Rather than relying on the measurement, Perea *et al* (2018) quantified the impact of urban climate on energy system design using a coupled CIM-CitySim model. CIM will provide the meteorological data as the inputs to drive CitySim to determine the energy demand of a district [23]. While Toparlar *et al* (2018) applied complex CFD to provide meteorological information for building energy simulation to estimate the impact of urban climate and parks on the summertime building cooling demand [24]. Santosa et al (2018) used Urban Weather Generator (UWG) to pre-process the urban EPW file and estimate the in a representative district in downtown Abu Dhabi (UAE) [25]. The other is two-way coupling where the building energy simulation is dependent on the urban climate data, and urban climate simulation needs inputs from buildings. To account for the building effects on urban air temperature and UHI/UCI, various models have been developed to predict the urban air temperature considering the interaction between building and its surrounding environment. These models either provide a two-way coupling of the building energy model (BEM) with the urban canopy model (UCM-BEM) [26-27] or with the Town Energy Balance (TEB) scheme (TEB-BEM) [28] or a lumped thermal parameter model [29]. The BEM in [28] applied the heat balance method to calculate the energy demand of a building which was considered as a single thermal zone representing the thermal inertia of various building levels by a generic thermal mass. The model accounted for heat conduction through the enclosure, infiltration, ventilation, solar radiation through the windows and internal heat gains. Bueno *et al.* [30] coupled a detailed building energy program - Energyplus [31] - with the Town Energy Balance (TEB) model [28] to exploit the advantages and overcome the drawbacks of both models. Miguel *et al.* [29] also used the Energyplus model to couple with a lumped thermal parameter model and estimated temperature and specific humidity in the near-surface urban environment. The lumped urban canopy model took into consideration of heat fluxes coming from the walls, windows, the air handling unit, the urban boundary layer, the sky, road, ground and vegetation. These current sophisticated building-urban coupling models are able to capture the main heat transfer process between buildings and the urban

environment [32], but they have relatively low computational efficiency. Most of them aim to predict the building energy consumption and the effect of waste heat emissions from HVAC systems on the urban environment assuming a constant indoor air temperature rather than the fluctuating indoor air temperature which is widely experienced in naturally-ventilated buildings.

As a complement to the complicated models mentioned above, this paper presents a lumped urban-building thermal coupling model based on the previous versions developed by Silva *et al.* [33] and Yang *et al.* [12]. The lumped model is limited in scope, but insightful in physics to better understand the controlling parameters contributing to both the indoor and outdoor air temperatures [12]. It also benefits from its greater simplicity and computational efficiency compared with other complex models (e.g. UCM-BEM). It is more suitable to use for optimizing the urban plan design and predicting the urban air temperature and finding out where and when a UHI and UCI can co-exist in the process of densification. Silva *et al.* [33] developed a simple lumped (i.e. zero-dimensional) thermal model to simplify the complex urban geometry as a unified entity and calculated the characteristic temperature of the entire urban area. Yang *et al.* [12] improved the lumped mesoscale urban air temperature model by setting up the heat balance equations for both urban air and urban surface and considering the heat exchange between them. But the lumped thermal model improved by Yang *et al.* [12] still assumed a constant indoor air temperature in air-conditioned buildings rather than a diurnally changing indoor air temperature. Moreover, the waste heat emissions from air-conditioning systems are integrated in the anthropogenic heat, not coupled with urban air temperatures.

In this paper, a lumped urban-building thermal coupling model is further developed to address the above-mentioned shortcomings, and verified using observational data from Hong Kong. The model is then used in a series of parametric analyses to investigate the effect of urban geometries (e.g., the increase of building density and building height) and internal heat gain on the urban air temperature and UHI/UCI intensity. In the meantime, the parameters such as urban air temperature and UHI/UCI intensity are compared between the cities with naturally-ventilated buildings and those with air-conditioned buildings. The model is also used to investigate the dominant mechanisms by which the time constant of a city affects urban air temperature and UHI/UCI intensity, and the reason why there is a difference in air temperature between the city with naturally-ventilated buildings and one with air-conditioned buildings. In addition, the asymmetry phenomenon of the diurnal urban air temperature which gives rise to the asymmetry warming is analysed. The outcomes of this

study can be used to guide the urban planning for designing cities that are more energy and environmentally resilient.

2. Numerical Simulation

2.1 Model Description

Fig.1 presents a sketch of the simplified city-building coupling model and two types of buildings: naturally-ventilated (NV) and air-conditioned (AC). In this model, the complex urban geometry is simplified as a lumped system. The average temperatures of all the effective thermal mass and surfaces are considered to be the same. The urban plan area (A_u) is the sum of the areas of vegetated surfaces A_v (such as plants and parks), artificial ground surfaces A_a (such as streets, highways and playgrounds) and roof surfaces A_p (equivalent to the building footprint). The total area (A_t) includes both the plan area (A_u) and the wall surface area of buildings (A_w). The relationships between the terms are shown in Equations (1), (2) and (3).

$$A_v + A_a + A_p = A_u \tag{1}$$

$$\lambda_v + \lambda_a + \lambda_p = 1 \tag{2}$$

$$A_t = A_u + A_w = (1+\lambda_w)A_u \tag{3}$$

where λ_v , λ_a , λ_p and λ_w are the respective area fractions of the four urban surfaces mentioned above. The idealized city (urban region) has the dimension $L \times L$. The plan-area-weighted average building height and the average distance between buildings are H and W, respectively. The urban control volume extends to the urban canopy layer height, which is shown in Fig.1.

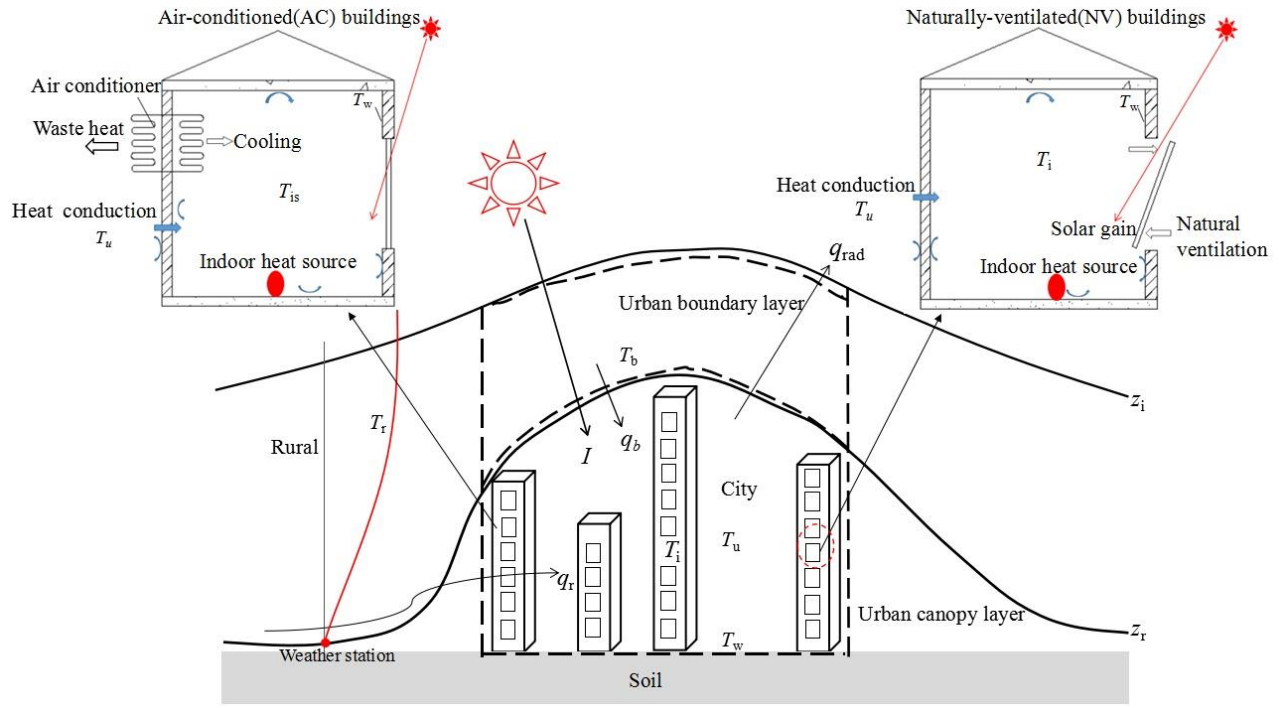

Figure 1: A sketch of the simplified urban-building coupling model

2.1.1 Models for an ideal city with naturally-ventilated buildings (NV case)

To obtain the dynamic evolution of the indoor air temperature in naturally-ventilated buildings as shown in Fig.1, the sensible heat balance for indoor air needs to be solved. The sensible heat balance is composed of the ventilation heat flux, the convective heat flux and the internal heat flux. The energy balance equation for the indoor air is presented as follows:

$$M_i C_i \frac{dT_i}{dt} = \rho c_p q_{iu}(T_u - T_i) + (U_r A_u + U_w A_w)(T_w - T_i) + E_i \lambda_p A_u N_{fl} \quad (4)$$

where $M_i C_i$ is the thermal mass of indoor air; T_i is the indoor air temperature; ρ is the air density; c_p is the specific heat of air; U_r and U_w are the U values of building roofs and walls， respectively； E_i is the internal heat source intensity (W/m^2), including heat from persons, lights, devices and solar through the windows; N_{fl} is the average number of building stories and q_{iu} is the natural ventilation rate, which will be discussed in more detail in section 2.2.

The heat balance for the urban air is composed of the advection heat flux from the rural site and the urban boundary layer, the ventilation heat flux from buildings, the convective heat flux and the anthropogenic heat flux. The governing equation for the urban air energy balance is shown in Eq. (5).

$$M_u C_u \frac{dT_u}{dt} = \rho c_p q_r (T_r - T_u) + \rho c_p q_b (T_b - T_u) + \rho c_p q_{iu} (T_i - T_u) + h_{co} A_t (T_w - T_u) + Q_{an} A_u \quad (5)$$

where $M_u C_u$ is the thermal mass of the urban air; h_{co} is the convective heat transfer coefficient between the external surface and the urban air, h_{co}=5.7+3.8v (v is the wind velocity) [34] and Q_{an} is the anthropogenic heat, which will be discussed in section 2.3; T_u, T_w, T_b, T_r are the canopy layer, surface, urban boundary layer and rural air temperatures, respectively; q_r, q_b are the volumetric flow rates flowing into the urban area from the rural-urban boundary layers, respectively, which have been discussed in [12]. The first, second and third terms of the right hand of Eq. (5) represent the heat flux from the rural-urban boundary layers and internal rooms by ventilation.

According to [35], the air temperature above the urban canopy layer T_b can be calculated by solving the heat balance of the urban boundary layer (UBL) model shown as follows:

$$V_{cv} \rho c_v \frac{dT_b}{dt} = H_{urb} + \int u_{ref} \rho c_p (T_{ref} - T_b) dA_f \quad (6)$$

where V_{cv} is the control volume; c_v is the specific heat of air at constant volume; c_p is the specific heat of air at constant pressure; H_{urb} is the sensible heat flux at the surface of the control volume (W); u_{ref} is a reference air velocity and A_f is the lateral area of heat exchange between the control volume and its surroundings. T_{ref} is a reference potential temperature outside the control volume, which is obtained by the vertical diffusion model (VDM) shown in the following equation.

$$\frac{dT_r(z)}{dt} = -\frac{1}{\rho(z)} \frac{\partial}{\partial z} [\rho(z) K_d(z) \frac{dT_r(z)}{dz}] \quad (7)$$

where z is the vertical height; K_d is the diffusion coefficient. The lower boundary condition of the vertical diffusion model is the temperature measured at the weather station $T_r(z_r)$. The upper boundary condition

accounts for the fact that at a certain height (z_{ref}~150 m), the profile of potential temperature is uniform and $(\partial T_r / \partial z)_{z_{ref}} = 0$. More details about T_b and T_r can be found in [35].

The heat balance for the surfaces is composed of the solar gain, the conductive heat flux, the convection heat flux, the evapotranspiration heat flux and the long-wave radiation heat flux to the sky. The energy balance equation for the surfaces becomes Eq. (8).

$$\begin{aligned}\sum \rho_i c_i \Delta x_i A_i \frac{dT_w}{dt} &= (1-\alpha)\ IA_u + k_v A_v \frac{T_{wx,v} - T_w}{\Delta x_v} \\ &+ k_a A_a \frac{T_{wx,a} - T_w}{\Delta x_a} + (U_r A_p + U_w A_w)(T_i - T_w) \\ &+ h_{co} A_t (T_u - T_w) - q_{evp} A_v - q_{rad} A_u\end{aligned} \tag{8}$$

where $\sum \rho_i c_i \Delta x_i A_i$ is the sum of the thermal mass of the wall and other surfaces and α represents the urban albedo, studied by Yang *et al.* [36]. The effective depth (Δx) is the depth into the ground or walls that can be reached by the diurnal temperature wave as used in the force-restore method. k_v and k_a are the conductivities of vegetated and man-made ground surfaces, respectively. $T_{wx,v}$ and $T_{wx,a}$ are the vegetated and man-made ground subsurface temperatures at effective depth Δx, respectively. q_{evp} and q_{rad} are the evapotranspiration heat flux and long-wave radiation heat flux to the sky, see [33]. More details can be found in Table 2 in the literature [12].

2.1.2 Models for an ideal city with air-conditioned buildings (AV case)

As shown in Fig.1, when the indoor air temperature is kept constant, T_i=$T_{is,}$ e.g. T_{is}=22°C, by air-conditioning systems, Eq. (4) becomes Eq.(9):

$$Q_l = \rho c_p q_{is} (T_u - T_{is}) + (U_r A_u + U_w A_w)(T_w - T_{is}) + E_i \lambda_p A_u N_{fl} \tag{9}$$

where Q_l is the cooling load of buildings; T_{is} is the indoor air temperature set point; q_{is} is the air change required for health; $q_{is} = ACH \times A_f \times H$ (*ACH* is the air change time (*ACH*=1.0h^{-1} in this paper).

When T_i=T_{is}, Eq. (10) is given as follows:

$$\begin{aligned}M_u C_u \frac{dT_u}{dt} &= \rho c_p q_r (T_r - T_u) + \rho c_p q_b (T_b - T_u) \\ &+ h_{co} A_t (T_w - T_u) + Q_{an} A_u + (1 + 1/COP) Q_l\end{aligned} \tag{10}$$

where *COP* is the coefficient of performance of the cooling system. The last term of the right hand of Eq. (10) is the waste heat of the air-conditioning system.

The energy balance equation for the surfaces becomes:

$$\begin{aligned}\sum \rho_i c_i \Delta x_i A_i \frac{dT_w}{dt} &= (1-\alpha)\ IA_u + k_v A_v \frac{T_{wx,v} - T_w}{\Delta x_v} \\ &+ k_a A_a \frac{T_{wx,a} - T_w}{\Delta x_a} + (U_r A_p + U_w A_w)(T_{is} - T_w) \\ &+ h_{co} A_t (T_u - T_w) - q_{evp} A_v - q_{rad} A_u\end{aligned} \tag{11}$$

2.2 Ventilation rates estimation

The air flowing into the urban area comes from three sources: the rural, the urban boundary layers and rooms. Yang *et al.* [12] have obtained the formula for the airflow rate (q_r) from the rural area and the airflow rate (q_b) from the urban boundary layers, shown in Eq. (12) and Eq. (13).

The airflow rate from the rural area (q_r) can be estimated as

$$q_r = \int_0^H (1-\lambda_p^{\frac{1}{2}}) L U \ln(\frac{z}{z_o}) dz / \ln(\frac{z_m}{z_o}) \tag{12}$$

where U is the velocity measured at height z_m at the rural station and z_o is the roughness length.

The airflow rate from the urban boundary layers (q_b) is

$$q_b = [(L - x_o)L](1-\lambda_p) U_E \tag{13}$$

where $x_o = 3L_c \ln K$ and L_c is the canopy drag-length scale. The term $\ln K$ varies between 0.5 and 2 for typical urban parameters [37].

Assuming that there is a large window in every room and natural ventilation is driven only by thermal force, the natural ventilation rate of the indoor region is calculated by Eq. (14).

$$q_{iu} = \frac{1}{3} C_d A_{wi} \sqrt{\frac{g H_{wi}(T_i - T_u)}{T_i}} \tag{14}$$

where C_d is the discharge coefficient; A_{wi} is the window area and H_{wi} is the height of window opening.

2.3 Anthropogenic heat estimation

Anthropogenic heat emissions result from various sources including human metabolism, industry, vehicles and buildings. Sailor *et al.* [38] found that human metabolism was generally a small component (~2-3%) of the total anthropogenic heating profile. In addition, there is few industry in Hong Kong [39]. Therefore, the anthropogenic heat generated from human metabolism and industry is ignored in current study. The heat flux generated from buildings is included in Eq. (5) and Eq. (10) according to Sailor *et al.* [40]. The heat flux generated from traffic in June, July and August accounts for about 44% of the total anthropogenic heat [41]. The total anthropogenic heat correlates well with population density. The greater population density in a city will result in greater anthropogenic heat. Sailor *et al.*[41] obtained the non-dimensional summer anthropogenic heating profiles for many cities and developed the predictive models for the maximum anthropogenic heat flux.

In summer, the predictive model of the maximum anthropogenic heat flux is shown in Eq. (15) according to the literature [41].

$$Q_{f\max} = \beta_0 + \rho_p \beta_1 \tag{15}$$

where ρ_p is the population density in persons per square kilometre, β_0 and β_1 are the coefficients for the regression models [41].

Sailor *et al.* [41] pointed out that the value of Q_{fmax} predicted by Eq. (15) may significantly overestimate anthropogenic heating in cities within other countries except the U.S. Eq. (16) was presented as follows

$$Q_{f\max}(non-U.S.) = f_{ec} Q_{f\max} \tag{16}$$

where f_{ec} is the relative energy consumption. f_{ec} =0.23 for Chinese cities [41].

In this study, the Kowloon Peninsula in Hong Kong (22º15'N,114º15'E) with an area of 47km^2 is selected as the target urban area. The population density of the Kowloon Peninsula is about 40,000 persons per square kilometre (2011 population census). Therefore, the maximum total anthropogenic heat flux is 64.9W/m^2 in summer according to Eq. (16) and the heat flux generated from the traffic is about 28.6W/m^2.

2.4 A new measure of urban heat island and urban cool island intensity

In this paper, the urban heat island degree hours (UHIdh) and the urban cool island degree hours (UCIdh) which were defined in [12] are used to measure how much (in degrees) and for how long (in hours) the urban

air temperature is lower/higher than the rural air temperature. As shown in Fig.2, UHIdh and UCIdh represent the area between the higher urban and lower rural air temperature and the area between the higher rural and lower urban air temperature, respectively. The formulae for UCIdh and UHIdh are shown as follows [12]:

$$UCIdh = \int_{t_{\min}}^{t_{\max}} (T_r(t) - T_u(t))dt \quad (17)$$

$$UHIdh = \int_{0}^{t_c} |T_r(t) - T_u(t)|\,dt - \int_{t_{\min}}^{t_{\max}} (T_r(t) - T_u(t))dt \quad (18)$$

where $t_{\min}$ and $t_{\max}$ are the start time and the end time when the urban air temperature is lower than the rural air temperature. t_c is the time period under consideration, 24h in this study.

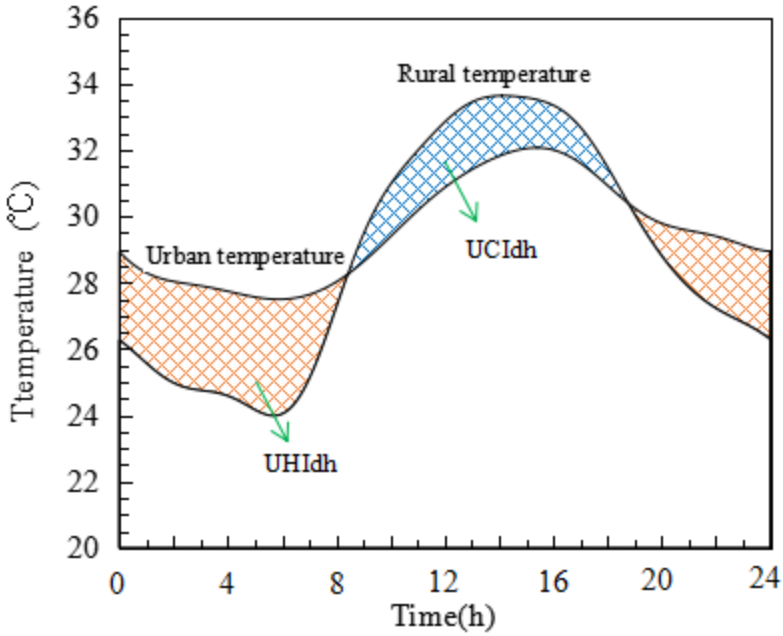

Figure 2: The definition of UCI degree hours and UHI degree hours

2.5. Model validation

The Kowloon Peninsula in Hong Kong has undergone rapid urbanization over the past 50 years, from a low-rise, low-density city to a high-rise, high-density city. Peng *et al.* [42] obtained the data for the changes in the three-dimensional urban morphology of Kowloon during the period 1964-2010 including building densities and heights. We assume there was no use of air-conditioning for 1960-1980 (NV case), with the AC case applying for 1988-2014. The Hong Kong Observatory (HKO, 22°18'N, 114°10'E) is the most representative urban station. The most representative rural station is the Ta Kwu Ling (TKL, 22°31'N,114°09'E) [43]. The average hourly data from 1960 to 1980 and from 1988 to 2014 of the Ta Kwu

Ling (TKL) and the Hong Kong Observatory (HKO) during the summer (June-August) are used to verify the results in the NV and AC cases, respectively. The data in calm (wind speed at the rural station was no more than 3m/s) and clear days (the cloud cover at the urban station was less than or equal to 2 Oktas) are selected. The selected method applied to the data is detailed in [12].

The fourth-order Runge-Kutta method is used to solve Eqs. (4), (5) and (8) for the NV case and Eqs. (9), (10) and (11) for the AC case. In order to obtain the valid comparative results between the two cases, the internal heat source intensity E_i in Eq. (4) must match with that in Eq. (9) to calculate the cooling load of buildings Q_l. The iteration time step is 36s. The input parameters of the Kowloon Peninsula are shown in Table 1. The average building height and density are given as the average values during 1960-1980 and 1988-2014. The building envelopes and the horizontal artificial area are made up of concrete and asphalt, respectively. Thermal properties for all materials are obtained from [44]. The diurnal anthropogenic heat profile followed the recommendation from [41] with the maximum anthropogenic heat flux for 1960-1980 and 1988-2014 calculated using Eqs. (15)-(16). Other parameters are detailed in [12]. Fig.3 and Fig.4 show the comparison between the observation and simulation for the NV and AC cases, respectively. Our simple model can predict the main features of the daily urban temperature cycle well for both the NV and AC cases. Table 2 also shows the Root Mean Squared Error (RMSE) and Mean Bias Error which quantify the absolute and bias errors between the simulation and observation. The RMSE and the mean bias error for the NV case are 0.94℃ and 0.47℃, while for the AC case they are 0.78℃ and 0.61℃, respectively. From Fig.3, the daily urban temperature cycle is postponed about two hours for the NV case, which results in an absolute error larger than 1.0℃ from 7:00-12:00. From Fig.4, the occurrence of the daily maximum urban temperature for the AC case is delayed by about two hours. The simulation results agree with the observation very well from 7:00-16:00. The larger discrepancy appears between 0:00-7:00 and between 16:00-24:00. Also, the predicted urban temperature is higher than the observations, indicating the model for the AC case overestimates the urban air temperature.

Table 1: The input parameters for modelling the urban air temperature in the Kowloon Peninsula in summer for comparison with the observed data.

Items	Settings

Location	Hong Kong
Study area	7km×7km
Simulation time-step	36s
Average building height	18m(NV) , 36m(AC)
Building density	0.21(NV), 0.32(AC)
Floor height	3m
Glazing-to-wall ratio	0.25
COP of the cooling system	2.5
Internal heat source	7.5W/m^2(fl)
Depth , heat capacity and U values of wall	0.3m; 2.11 ×10^6J/(m^3·K); 1.7W/(m·K)
Depth, heat capacity and U values of roof	0.2m; 1.94×10^6J/(m^3·K); 0.5W/(m·K)
Depth, heat capacity and heat conductivity of pavement ground	0.2m; 1.94×10^6J/(m^3·K); 0.75W/(m·K)
Depth, heat capacity and heat conductivity of natural ground	0.1m; 1.42×10^6J/(m^3·K); 0.25W/(m·K)
Temperature at the effective depth **below ground level**	20℃
Indoor air temperature set-point	22℃
Evapotranspiration for green **areas**	2.0 ×10^{-7}m/s

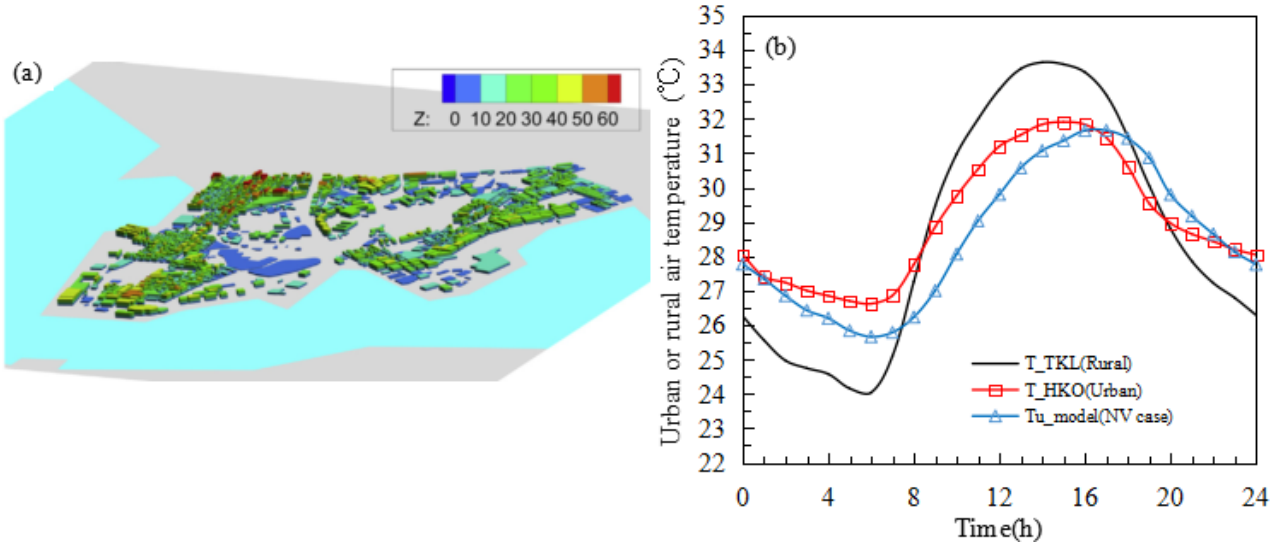

Figure 3: Comparison between the observed and calculated urban air temperature for the NV case

((a) Urban Kowloon in 1980 [42])

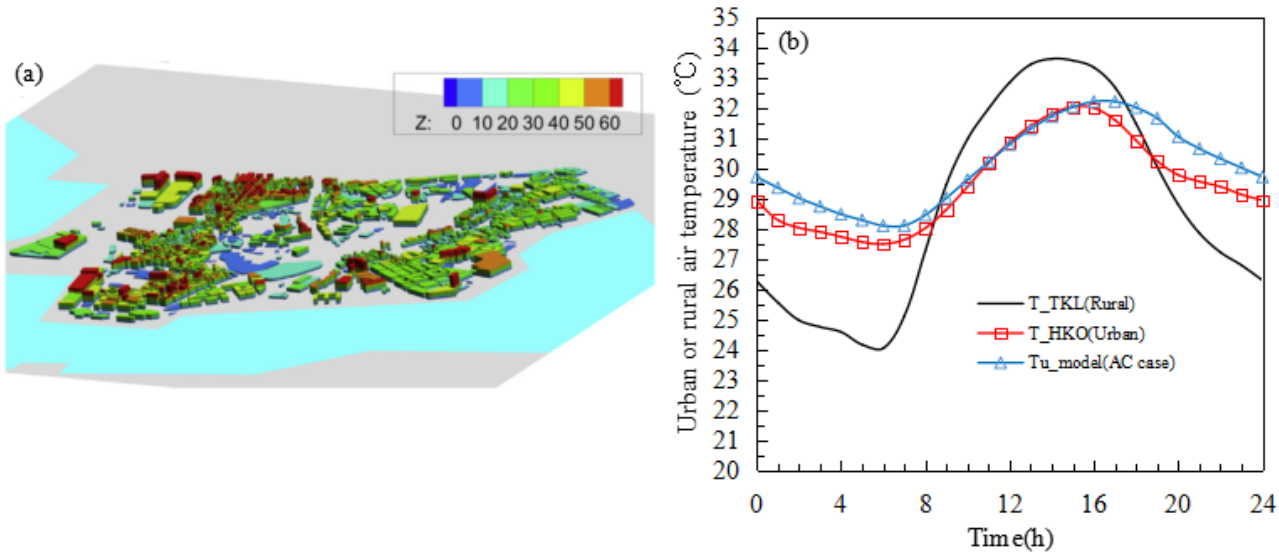

Figure 4: Comparison between the observed and calculated urban air temperature for the AC case

((a) Urban Kowloon in 2010 [42])

Table 2: The Root mean square error (RMSE) and mean bias error (MBE) of the comparison between the observed and calculated data

Case type	Statistics	Numerical solution
NV case	Root-mean-square error (℃) RMSE	0.94
	Mean bias error (℃) MBE	0.47
AC case	Root-mean-square error (℃) RMSE	0.78
	Mean bias error (℃) MBE	0.61

2.6 Scenario description for urban densification

To further investigate the impact of urban densification (i.e. the growth and evolution of the city in our case), we take into account various urban scenarios. We assume the buildings in a city are homogenously distributed. Table 3 shows the urban morphological details of all scenarios. The urban morphology illustrates the evolution from a low-rise, low-density city to a high-rise, high-density city. In the lumped thermal systems, the time constant is an important parameter which characterizes the response to the temperature variation of the environment temperature [12], depending on the thermal storage capacity of a city and the ventilation. The surface characteristics and environmental input data are the same as in Table 1.

Table 3: The urban scenarios

Low density（λ_p =0.16）		Medium density（λ_p =0.25）		High density （λ_p =0.49）	
H/*W*	τ	*H*/*W*	τ	*H*/*W*	τ
0.5	1.95	0.5	2.20	1	6.45
0.875	3.71	1	4.90	2	11.89
1	4.12	2	8.12	3	16.33
1.5	5.52	3	10.41	4	20.18
2	6.59	4	12.04	5	23.46
3	7.95	5	13.23	6	26.26
4	8.92	7	14.80	8	30.75
6	10.04	10	16.08	10	34.13
8	10.62	12	16.57	12	36.73
10	10.95	15	17.02	20	42.74

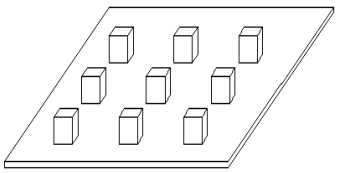

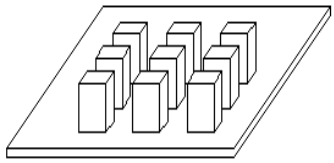

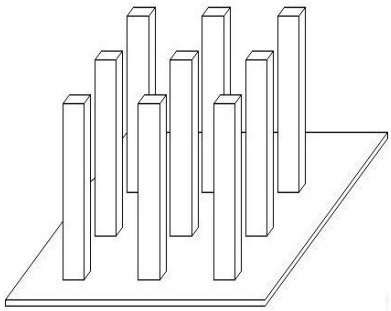

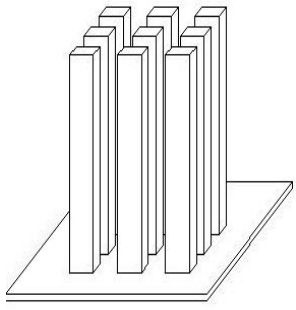

3. Results and Discussions

3.1 The diurnal urban air temperature cycle and its asymmetry: naturally-ventilated vs. air-conditioned buildings

The diurnal urban air temperature profiles for the AC and NV cases for the low-rise, low-density city (λ_p =0.16, H=15m) and the high-rise, high-density city (λ_p =0.49, H=60m) are shown in Fig. 5. The internal heat source intensity is maintained as constant at 7.5W/m^2(fl), which is the representative internal heat intensity for a Chinese household.

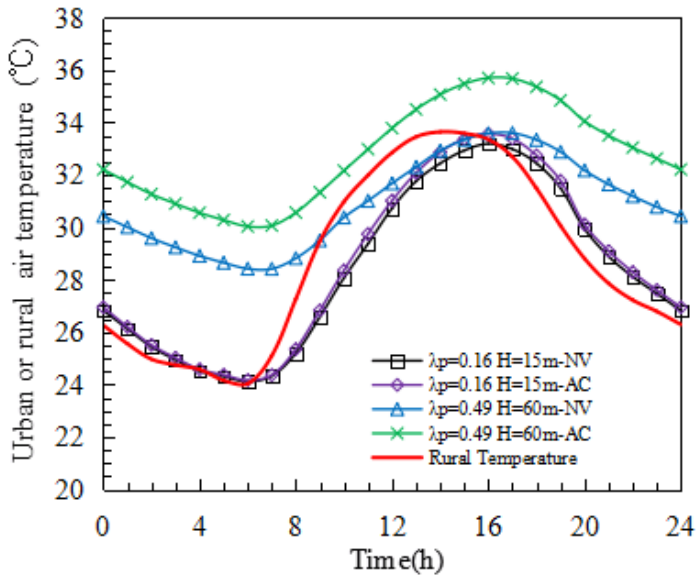

Figure 5: The urban air temperature comparison between the AC and NV cases

The urban air temperature for the NV case is generally lower than that when the indoor air temperature is kept constant by air-conditioning systems (AC case) for all urban scenarios. It is also at the cost of elevated indoor air temperature and sacrificing indoor thermal comfort for the NV case. This implies that waste heat emissions from the air-conditioning system have more influence on the urban air temperature than the indoor-outdoor heat exchange by ventilation only when the other conditions keep the same. Comparing Eq. (5) with Eq. (10), it can be deduced that the urban air temperature in the AC case is higher than that in the NV case because the sum of the condensation heat of the air-conditioning system and the convection heat between the external surface and the urban air in the AC case (called Q_{AC}) is larger than the sum of the indoor-outdoor air heat exchange and the convective heat transfer in the NV case (called Q_{NV}). When the indoor air temperature is kept constant by air-conditioning systems (the AC case), the heat exchange between the indoor and urban environments includes the condensed sensible heat of the air-conditioning system and the heat transfer through

the building envelopes. When the indoor and urban air temperatures are non-linearly coupled (the NV case), the heat exchange between the indoor and urban environments is produced only by air exchange and heat transfer through the building envelopes. In addition, the urban air temperature difference between the two cases becomes larger when the building density and building height increase. For the low-rise, low-density city (λ_p =0.16, H=15m), the urban air temperature difference between the two cases is very small (<0.5℃). While for the high-rise, high-density city (λ_p =0.49, H=60m), the urban air temperature difference becomes 1.5℃-2.5℃. With the process of urban densification, the urban warming attributable to the use of air-conditioning systems is becoming more dominant.

Furthermore, both of the spatial and temporal asymmetry phenomena in the daily urban temperature cycle [45] are also observed in Figure 5. On the one hand, when a city grows from a low-rise, low-density one to a high-rise, high-density one, the mean urban air temperature increases but the amplitude decreases, leading to a much faster rise in the daily minimum urban temperature than that of the maximum urban temperature. This phenomenon is called the temporal asymmetry [45] which brings about temporal asymmetry warming, i.e. a much faster increase in the urban temperature during the night time than that in the daytime, as shown in Fig.5. Therefore, the UHI becomes more predominant, while the UCI becomes weaker during the process of urbanization and, finally, UCI disappears for the high-rise high-density city in the AC case (green line in Figure 5).

On the other hand, when the urban air temperature is compared with the rural air temperature, the spatial asymmetry phenomenon occurs. The reasons underlying the spatial asymmetry phenomenon include the clear phase delay except for the increasing mean urban temperature and the decreasing diurnal temperature range. The urban air temperature shows a phase delay of 1~3 hours with respect to the rural air temperature. The spatial asymmetry phenomenon becomes more noticeable with the increase in the building density and height. The combination of the spatial and temporal asymmetry phenomena can explain why the urban heat island effect is stronger in the night time than that during the daytime or why the urban heat island appears in the night time while the urban cool island exists in the daytime. It can also give the reason why the high-rise, high-density city experiences a stronger heat island effect and weaker cool island effect, which differs from the results obtained by Yang *et al.* [12]. Such different results are due to the fact that no anthropogenic heat and

condensation heat from the air-conditioning system are considered by Yang *et al.* [12]. Moreover, Fig.5 also shows that the diurnal asymmetry warming phenomenon in the AC case is more obvious than that in the NV case, especially for a high-rise, high-density city.

3.2 Parametric analysis of the effect of urban morphology and internal heat gain on UCIdh and UHIdh

As mentioned in section 2.6, the time constant gives expression to the thermal storage capacity and air flow rate, both of which are related to the urban morphology. The time constant quantifies the effective thermal storage. The total internal heat gain of buildings is also related to the urban morphology for the given internal heat intensity which affects the urban-building heat exchange (the denser and higher the buildings are, the more internal heat gain there could be). The UCIdh and UHIdh mentioned in section 2.4 measure how much and for how long the urban air temperature is lower/higher than the rural air temperature [12].

Figs.6~7 illustrate the relationship between the UCIdh, UHIdh and the time constant under different building densities and internal heat intensities for both AC and NV cases. The results are derived from all the cases shown in Table 3.

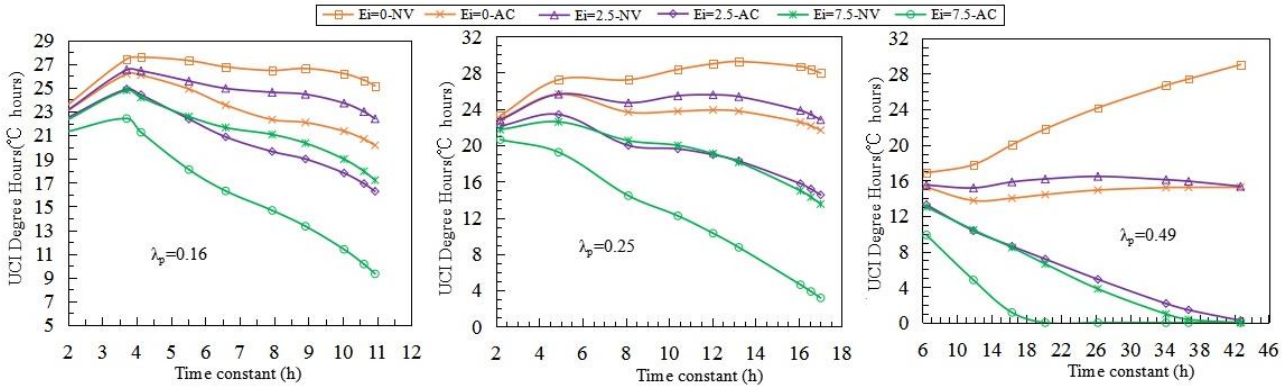

(a) λp=0.16 (b) λp=0.25 (c) λp=0.49

Figure 6: Relationship between the UCIdh and the time constant for the NV and AC cases

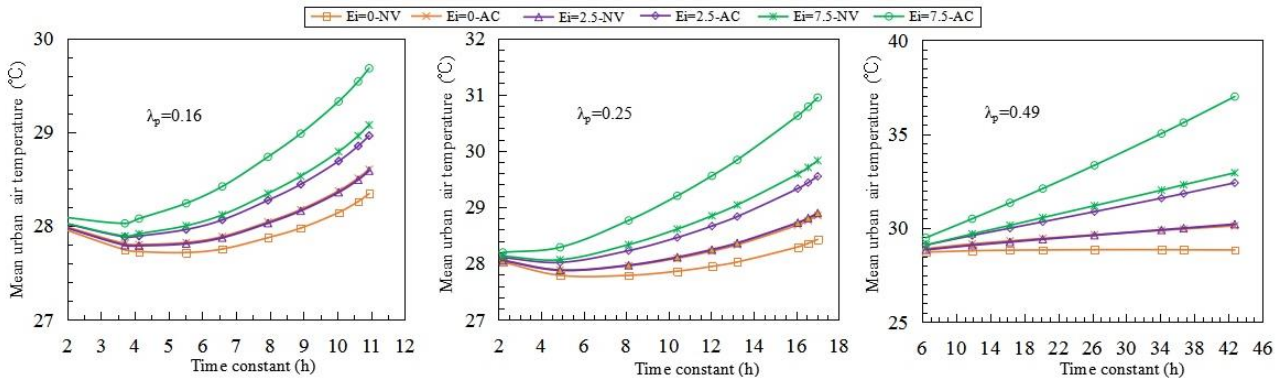

(a) λp=0.16 (b) λp=0.25 (c) λp=0.49

Figure 7: Relationship between the UHIdh and the time constant for the NV and AC cases

As shown in Figs. 6(a) and 7(a), for a low-density city (λ_p =0.16), UCIdh first increases rapidly, reaching the maximum value and then decreases when the time constant further increases. On the contrary, UHIdh first declines slowly, and then increases sharply. Comparing Fig.6(a) with Fig.7(a), it should be noted that the maximum UCIdh appears when the time constant is 3.71-4.12(H/W = 0.875~1) and the minimum UHIdh exists when the time constant is 3.71-5.52(H/W =0.875~1.5). This can be explained by the fact that the heat storage capacity due to human-made structures, such as buildings and roads, firstly exceeds the internally generated heat when the time constant is low (an UCI exists). The time lag due to heat storage also plays a role. When the stored heat is equal to the heat generation, the UCIdh achieves the maximum value. This is also reflected by the fact that the mean urban air temperature firstly declines slightly and then increases, as shown in Fig.8(a), and the amplitude of the urban air temperature shrinks as the time constant increases, as shown in Fig.9(a). However, the maximum and minimum air temperatures do not change in synchrony, i.e. the maximum temperature in the daytime decreases at a higher rate compared with the slow increase of minimum temperature at night when the time constant is smaller than 4. This leads to a decrease in the mean air temperature (see Figure 8(a)). While the time constant further increases, the rate of increase of the minimum air temperature surpasses the rate of decrease of the maximum air temperature leading to an obvious asymmetry of the urban air temperature cycle as mentioned in [45] and also in Section 3.1. The asymmetry warming phenomenon becomes more obvious as the time constant and internal heat gain rise further.

When the building density λ_p = 0.49 (a high-density city), both UCIdh and UHIdh increase as the time constant becomes larger for naturally-ventilated buildings with zero internal heat gain (see Figs. 6(c)-7(c)), which agrees with the results in [12]. This is explained by the fact that the amplitude of the urban air temperatures will decrease under urbanization (the increase of the time constant) shown in Fig.9(c), but the mean urban air temperature, as shown in Fig.8(c), increases slightly and an increase in the daily minimum temperature is almost equal to a decrease in the daily maximum temperature. The approximate symmetry phenomenon of the diurnal urban temperature (Fig.1(c) in the literature [45]) appears. But for a city with air-conditioned buildings, much more waste heat from air-conditioning systems will be released into the atmosphere in spite of there being no internal heat gain (E_i=0 for AC), which violates the symmetry phenomenon and leads to the asymmetry of the diurnal urban temperature, thus the UCIdh first decreases and then slightly increases as the time constant increases. The operation of the building, i.e. either natural ventilation or air conditioning, has a significant impact on the urban climate under urban densification. When the internal heat source intensity increases to 2.5 and 7.5W/m^2 (more internal heat gain), the UCIdh decreases to zero and the UHIdh increases rapidly due to much more heat being released to the urban environment than that being stored by human-made structures. In addition, the difference between the minimum urban temperature and the minimum rural temperature (maximum urban heat island intensity) is much larger than that between the maximum urban temperature and the maximum rural temperature, as shown in Fig.9(c). This is consistent with the studies of Wang *et al.* [45] and Oke [46] which have found that the temperature difference between urban and rural is usually larger during the night than in the day. When the building density λ_p = 0.25 (a medium-density city) and the internal heat source intensity increases to 7.5W/m^2 in a city with air-conditioned buildings, the UCIdh decreases and the UHIdh increases as the time constant increases, which is different from the result for λ_p=0.16 (Figs. 6(b)-7(b)). Otherwise, the variations in both the UCIdh and UHIdh are observed to be similar to that for λ_p=0.16.

Figs. 6~9 also highlight the important impact of the total internal heat gain (either due to the increase of internal heat gain intensity or due to the increase in the total floor area under urbanization). The heat released from the indoor environment to the urban environment increases with the increase of the total building internal heat gain, leading to an increase of the mean, maximum and minimum urban air temperatures shown in Figs.

8 and 9, therefore, the UCIdh declines and the UHIdh increases as the internal heat source intensity increases for the same time constant. But the internal heat gain has little impact on the amplitude and phase shift of the urban air temperature.

As can be seen from Figs. 6~7, the UCIdh for the NV case is larger than that for the AC case. In contrast, the UHIdh for the NV case is smaller than that for the AC case. Moreover, the UCIdh and UHIdh for the NV case changes slower than in the AC case. The UCIdh /UHIdh difference between two cases becomes larger as the building height and density increase. In addition, Fig.6 and Fig.7 also indicate that the UCIdh decreases and UHIdh increases in the process of urbanization (as the building density and height increase). It can be deduced that the UCI and UHI co-existing phenomena will disappear when the time constant increases to a certain value. These results can explain why urbanization produces a higher urban air temperature and a more intense UHI effect.

Comparing Figs. 6~7 with the results in [12], there are two factors that lead to the deviation between them. One reason is that no anthropogenic heat from buildings was considered in [12] and buildings act as a heat sink for the majority of the time as the internal temperature set-point is lower than the outdoor air temperature. The other reason is that the waste heat from air-conditioning systems relative to the urban air temperature was not calculated in the heat balance equation for the urban air temperature in [12]. Moreover, the waste heat from the air-conditioning systems relative to the urban air temperature still affects the amplitude and the delay time.

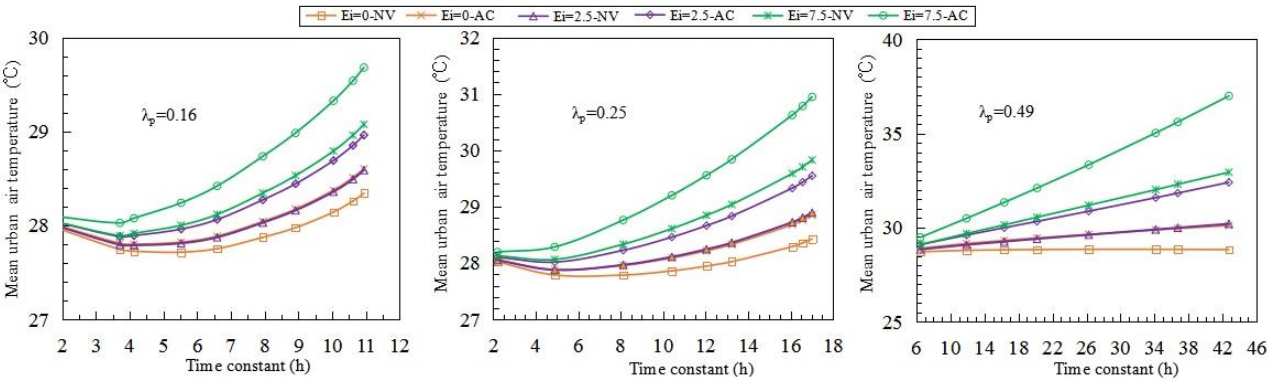

(a) λp=0.16 (b) λp=0.25 (c) λp=0.49

Figure 8: Relationship between the mean urban temperature and the time constant for the NV and AC cases

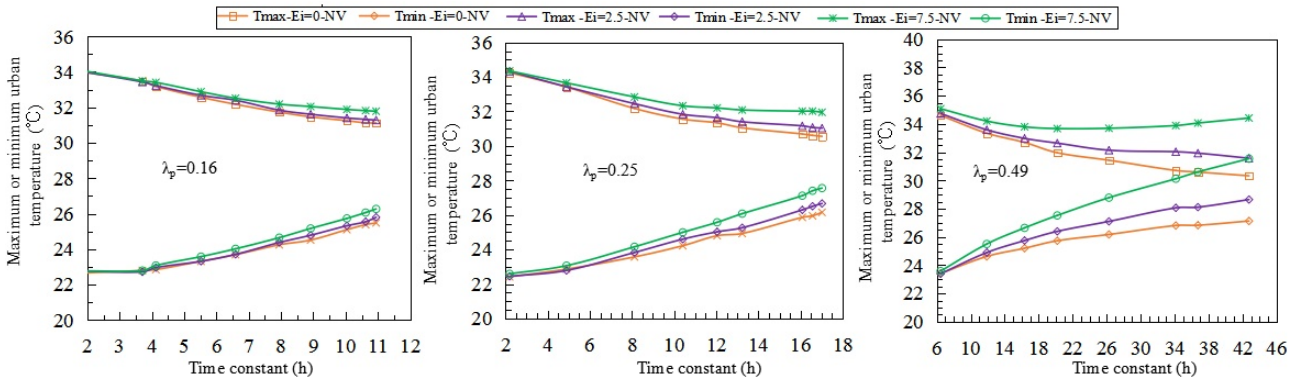

(a) λp=0.16 (b) λp=0.25 (c) λp=0.49

Figure 9: Relationship between the maximum and minimum urban temperatures and the time constant for the NV case

The above results show some special examples in the application of the lumped urban-building coupling model. In fact, the model can be used to estimate the urban air temperature and UHI/UCI intensity according to urban morphology and buildings operation modes in the initial stage of urban planning. The simulated results can be used as a guide to optimize the urban planning and design. The model is also applied to predict the natural ventilation potential and hourly energy consumption in existing cities, which helps to optimize the energy planning for existing cities.

4. Conclusions

A lumped urban-building thermal coupling model has been developed to predict the urban air temperature and urban cool island/urban heat island intensity in cities with naturally-ventilated buildings and air-conditioned buildings. Both the indoor-outdoor heat exchange by natural ventilation and the waste heat emissions from air-conditioning systems are considered. The urban-building thermal coupling model is able to capture the main features of the urban air temperature, including the coexistence of the urban cool island and urban heat island phenomena, but with a very low computational cost.

The model is then used to investigate the diurnal urban air temperature and its asymmetry for a city with naturally-ventilated buildings and one with air-conditioned buildings and the mechanism involved. The model predicts a lower urban air temperature and higher urban cool island intensity in a city with naturally-ventilated buildings (the NV case) than in a city with air-conditioned buildings (the AC case). For a low-rise, low-density

city, there is a very small difference in the urban air temperature between the two cases. But the difference increases under the scenario of urbanization/densification (increase of building height and density). This can be explained by waste heat emissions from air-conditioning systems having a greater influence on the urban air temperature than the indoor-outdoor heat exchange by ventilation. Moreover, the influence becomes remarkable for a high-rise or high-density city. Our simulation results could explain why urbanization produces a higher urban air temperature and more intense urban heat island effect. The asymmetry of the diurnal urban air temperature gives rise to the asymmetric warming phenomena, which become more obvious in a city with air-conditioned buildings than in a city with naturally-ventilated buildings as the time constant and internal heat gain increase.

The model is also used for a series of parametric studies to investigate the effect of urban geometries (described as the time constant) and internal heat gain on the urban air temperature and urban cool island/urban heat island degree hours in the process of urbanization. Urban cool island/urban heat island degree hours as defined in [12] offer a comprehensive measure of the urban cool/heat island intensity. Compared with the results in [12], the urban cool island/urban heat island degree hours (UCIdh/UHIdh) show different variation features. Generally speaking, a low-rise, low-density city experiences more urban cool island degree hours than a high-rise, high-density city under the same internal heat source intensity. For a low-density city, the urban cool island degree hours first increase and then decrease with the time constant increasing. For a high-density city, the urban cool island degree hours generally decrease as the time constant increases when the internal heat source intensity is not zero. The urban cool island degree hours decrease and urban heat island degree hours increase as the building density increases in the process of urbanization. These results imply that the urban cool island effect will disappear when the time constant increases to a large value and that urban cool island degree hours is an important parameter to affect the energy consumption of buildings.

Given its simplicity and high computational efficiency, the lumped urban-building thermal coupling model can be a useful tool for urban planners to predict urban cool/heat island intensity and for building engineers to predict building energy consumption or indoor air temperatures by introducing the interactions between buildings and the urban environment.

Acknowledgement

This study is financially supported by UK Natural Environmental Research Council (NERC) (NE/S005889/1). Shuangping Duan would like to acknowledge the financial support from the China Scholar Council (CSC) for the academic visit at the University of Reading and the Scientific Foundation of the Sichuan Education Department (12zb332).

References

[1] KC Seto, B Güneralp, LR Hutyra (2012). Global forecasts of urban expansion to 2030 and direct impacts on biodiversity and carbon pools. Proc. Natl. Acad. Sci. France 109 (40): 16083-88

[2] WTL Chow , M Roth (2006). Temporal dynamics of the urban heat island of Singapore. Int J Climatol 26(15):2243-2260.

[3] T Houet , G Pigeon (2011). Mapping urban climate zones and quantifying climate behaviors e an application on Toulouse urban area (France). Environ Pollut 159(8):2180-2192.

[4] ML Imhoff , P Zhang , RE Wolfe , L Bounoua (2010). Remote sensing of the urban heat island effect across biomes in the continental USA. Remote Sens. Environ. 114(3):504–513.

[5] M Kolokotroni , R Giridharan (2008). Urban heat island intensity in London: an investigation of the impact of physical characteristics on changes in outdoor air temperature during summer. Sol. Energy 82(11) : 986–998

[6] R Giridharan , M Kolokotroni (2009).Urban heat island characteristics in London during winter, Sol. Energy 83(9): 1668–1682

[7] M Santamouris (2015). Analyzing the heat island magnitude and characteristics in one hundred Asian and Australian cities and regions. Science of the Total Environment 512–513: 582–598

[8] CM Frey, G Rigo, E Parlow, A Marçal (2005). The cooling effect of cities in a hot and dry environment.Global developments in environmental earth observation from space : proceedings of the 25th EARSeL symposium, Porto, Portugal: 169–174.

[9] AL Chen , XA Yao , RH Sun , LD Chen(2014). Effect of urban green patterns on surface urban cool islands and its seasonal variations. Urban Forestry & Urban Greening 13(4): 646–654

[10] A Rasul , H Balzter , C Smith(2015). Spatial variation of the daytime Surface Urban Cool Island during the dry season in Erbil, Iraqi Kurdistan, from Landsat 8. Urban Climate 14: 176–186

[11] T Martins, L Adolphe, M Bonhomme, F Bonneaud, S Faraut, S Ginestet, C Michel, W Guyard (2016). Impact of Urban Cool Island measures on outdoor climate and pedestrian comfort: Simulations for a new district of Toulouse, France. Sustainable Cities and Society, 26: 9–26.

[12] X Yang, Y Li, Z Luo, PW Chan (2017). The urban cool island phenomenon in a high-rise high-density city and its mechanisms. Int J Climatol 37:890-904.

[13] P Cohen, O Potchter, A Matzarakis(2012). Daily and seasonal climatic conditions of green urban open spaces in the Mediterranean climate and their impact on human comfort. Build. Environ. 51:285–295

[14] S Hamada, T Ohta(2010). Seasonal variations in the cooling effect of urban green areas on surrounding urban areas. Urban Forestry & Urban Greening 9 (1):15–24.

[15] M Kolokotroni, I Giannitsaris, R Watkins(2006).The effect of the London urban heat island on building summer cooling demand and night ventilation strategies.Solar Energy 80(4): 383-392

[16] M Kolokotroni, X Ren , M Davies , A Mavrogianni (2012). London's urban heat island: impact on current and future energy consumption in office buildings. Energy and Buildings 47: 302-311

[17] Y Kikegawa, Y Genchi, H Kondo, K Hanaki(2006). Impacts of city-block-scale countermeasures against urban heat island phenomena upon a building's energy-consumption for air conditioning. Appl. Energy 83(6): 649–668.

[18] C Sarrat , A Lemonsu , V Masson , D Guedalia (2006). Impact of urban heat island on regional atmospheric pollution. Atmospheric Environment 40(10):1743-1758.

[19] B Bueno , G Pigeon , LK Norford , K Zibouche (2012).Development and evaluation of a building energy model integrated in the TEB scheme. Geosci. Model Dev.4(4): 2973–3011 .

[20] V Heidt, M Neef(2008). Benefits of urban green space for improving urban climate. Ecology, Planning, and Management of Urban Forests. Springer, New York： 84-96

[21] U Berardi, AH GhaffarianHoseini, A GhaffarianHoseini (2014). State-of-the-art analysis of the environmental benefits of green roofs. Applied Energy 115(4):411–428.

[22] M Zinzi ,E Carnielo ,B Mattonia(2018).On the relation between urban climate and energy performance of buildings. A three-years experience in Rome, Italy. Applied Energy 221: 148-160

[23] A.T.D.Perera, S Coccolo, JL Scartezzini, D Mauree(2018).Quantifying the impact of urban climate by extending the boundaries of urban energy system modeling. Applied Energy 222(15): 847-860

[24]Y.Toparlar,B.Blocken, B.Maiheu, G.J.F.van Heijst(2018).Impact of urban microclimate on summertime building cooling demand: A parametric analysis for Antwerp, Belgium. Applied Energy 228: 852-872

[25]LGR Santosa,A Afshari, L K.Norford, J Mao(2018).Evaluating approaches for district-wide energy model calibration considering the Urban Heat Island effect. Applied Energy 215: 31-40

[26] Y Kikegawa , Y Genchi , Y Yoshikado , H Kondo (2003). Development of a numerical simulation system for comprehensive assessments of urban warming countermeasures including their impacts upon the urban buildings' energy-demands. Appl. Energy 76: 449–466.

[27] H Kondo, Y Genchi, Y Kikegawa, Y Ohashi, H.Yoshikado, H Komiyama (2005). Development of a multi-layer urban canopy model for the analysis of energy consumption in a big city: Structure of the urban canopy model and its basic performance. Bound.-Layer Meteor. 116: 395–421.

[28]V Masson , CSB Grimmond , TR Oke (2002). Evaluation of the town energy balance (TEB) scheme with direct measurements from dry districts in two cities. J Appl Meteorol 41:1011–1026.

[29] M Miguel, A Afshari , PR Armstrong, LK Norford (2015). Estimation of urban temperature and humidity using a lumped parameter model coupled with an EnergyPlus model. Energy and Buildings 96: 221–235.

[30] B Bueno · L Norford · G Pigeon ·R Britter (2011). Combining a Detailed Building Energy Model with a Physically-Based Urban Canopy Model. Boundary-Layer Meteorol 140(3):471–489.

[31] DB Crawley, LK Lawrie , FC Winkelmann , WF Buhl , YJ Huang , CO Pedersen , RK Strand, RJ Liesen, DE Fisher, MJ Witte, J Glazer(2001). Energyplus: creating a new-generation building energy simulation program. Energy and Build 33(4):319-331.

[32] T Ihara , Y Kikegawa , K Asahi , Y Genchi , H Kondo (2008). Changes in year-round air temperature and annual energy consumption in office building areas by urban heat-island countermeasures and energy-saving measures. Applied Energy 85(1):12-25.

[33] HR Silva , R Bhardwaj , PE Phelan , JS Golden, S GrossmanClarke(2009). Development of a zero-dimensional mesoscale thermal model for urban climate. J. Appl. Meteorol. Climatol. 48(3): 657–668.

[34] W.H. Mcadams(1994), Heat Transmission(the 3rd edition). McGraw-Hill, New York.

[35] B Bueno , J Hidalgo, G Pigeon, L Norford , V Masson(2013). Calculation of air temperatures above the urban canopy layer from measurements at a rural operational weather station. J. Appl. Meteorol. Climatol. 52(2):472-483.

[36] X Yang, Y Li (2015).The impact of building density and building height heterogeneity on average urban albedo and street surface temperature. Building and Environment 90(8): 146-156

[37] O Coceal , SE Belcher (2005). Mean winds through an inhomogeneous urban canopy. Bound.-Layer Meteorol. 115(1):47-68.

[38] DJ Sailor, L Lu, H Fan(2003). Estimating urban anthropogenic heating profiles and their implications for heat island development. Fifth International Conference on Urban Climate, Lodz, Poland.

[39] WS Tang, JWY Lee, MK Ng (2012). Public engagement as a tool of hegemony: The case of designing the new central harbour front in Hong Kong. Critical Sociology 38(1): 89-106.

[40] DJ Sailor (2011). A review of methods for estimating anthropogenic heat and moisture emissions in the urban environment. International Journal of Climatology, 31(2), 189-199.

[41] DJ Sailor , M Georgescu , JM Milne , MA Hart (2015). Development of a national anthropogenic heating database with an extrapolation for international cities. Atmos. Environ. 118:7-18

[42] L Peng, JP Liu, Y Wang, PW Chan, TC Lee, F Penge, Ms Wong,Y Li (2018). Wind weakening in a dense high-rise city due to over nearly five decades of urbanization. Building and Environment 138(6): 207-220.

[43] WS Leong, MA Hart(2013).Quantifying urban heat island intensity in Hong Kong SAR, China. Environmental Monitoring and Assessment 185(5):4383–4398.

[44] TR Oke.(1987). Boundary Layer Climates, 2nd edn. Routledge: London & New York, 435.

[45] K Wang , Y Li , Y Wang, X Yang (2017). On the asymmetry of the urban daily air temperature cycle. Journal of Geophysical Research: Atmospheres 122(11):5622-5634

[46] TR Oke (1982). The energetic basis of the urban heat island, Q. J. R. Meteorol. Soc., 108(455): 1–24.